

## A Step Toward Production of Smaller Diameter Single Wall Carbon Nanotubes

V. Lemos<sup>a\*</sup>, D. Silva<sup>b</sup>, C.A. Luengo<sup>c</sup>, J.G. Huber<sup>d</sup>, J.M. Rosolen<sup>e</sup>

<sup>a</sup>*Departamento de Física, Universidade Federal do Ceará  
C.P. 6030, Campus do Pici, 60455-760 Fortaleza - CE, Brazil*

<sup>b</sup>*Instituto de Geociências, Universidade Estadual de Campinas  
13083-970 Campinas - SP, Brazil*

<sup>c</sup>*Instituto de Física, Universidade Estadual de Campinas  
13083-970 Campinas - SP, Brazil*

<sup>d</sup>*Independent researcher, 501 N. Boulevard, #7, Richmond - VA 23220, USA*

<sup>e</sup>*Departamento de Química, FFCLRP, Universidade de São Paulo  
14040-901 Ribeirão Preto - SP, Brazil*

Received: January 02, 2002; Revised: September 30, 2002

Single-wall carbon nanotubes were produced with, either, a bimetallic or a mixture of three catalysts. Raman scattering and high resolution transmission electron microscopy were used as characterization tools. The mixture  $\text{LiNi}_{0.5}\text{Co}_{0.5}\text{O}_2$  led to a sample relatively free from impurities with long bundles, each containing a few tubes. A narrow distribution of diameters for the sample produced with this mixture was evidenced by Raman scattering experiences. The mean tube diameter was found to be smaller than those measured for the nanotubes obtained with the bimetallic catalysts, Fe/Ni and Ni/Co. Possible chiralities were calculated for the semiconductor nanotubes formed. Assignments of the Raman radial breathing mode frequencies to the calculated structures are presented.

**Keywords:** *single-wall carbon nanotubes, raman scattering, high resolution transmission electron microscopy.*

### 1. Introduction

A great progress has been achieved in the growth mechanisms of single wall carbon nanotubes (SWCNTs) aiming, markedly, large scale production at low cost. The synthesis based on arc-discharge<sup>1-3</sup>, laser vaporization<sup>4</sup>, and gas-phase thermal decomposition<sup>5</sup>, have been reported extensively. All three methods need catalyst addition to carbon powder for yielding SWCNTs. Attempts in controlling the diameter distribution relied mainly in the choice of the catalysts. The tube diameter distribution change with the type of catalyst or the ratio of catalysts in a mixture<sup>6,7</sup>. The precursor catalysts used to generate SWCNTs were single transition metal such as Fe<sup>1</sup>, Co<sup>2</sup> and Ni<sup>3</sup>. Further on, the introduction of bimetallic catalysts, such as Co/Ni<sup>8</sup>, Fe/Ni<sup>8</sup>, Pt/Rh<sup>9</sup> and Ni/Y<sup>10</sup> were found effective in generating SWCNTs with high yield. Ni/Y, among those, is the SWCNTs mass production catalyst by arc-discharge. However, it is not clearly

understood why such a bimetallic combination is better than the single metal, especially for Y, itself, being not efficient to yield SWCNTs<sup>6</sup>. Therefore, to acquire the knowledge to improve diameter control and the formation of the tubes, it is necessary to investigate the role of the catalysts in detail.

Here, we describe the growth of SWCNTs by the arc-discharge process using the bimetallic catalysts Fe/Ni, Ni/Co, and the catalyst mixture of  $\text{LiNi}_{0.5}\text{Co}_{0.5}\text{O}_2$ . High Resolution Transmission Electron Microscopy (HRTEM) was employed to observe the morphology of the sample as well as the dimensions of the bundles of nanotubes formed. The mean diameter of the SWCNTs measured in this way was of 1.46 nm for the sample prepared with the  $\text{LiNi}_{0.5}\text{Co}_{0.5}\text{O}_2$  as catalyst. The micro Raman technique was employed in two ways, to probe the tubes abundance using the tangential modes, and to measure the sub-set diameter distribution through the radial breathing modes (RBMs). The low frequency spectra taken from different samples, were found to

\*e-mail: volia@ifi.unicamp.br

differ appreciably. It was found, for instance, that the RBMs for excitation in the blue,  $E = 2.54$  eV, peak at  $158\text{ cm}^{-1}$ ,  $180\text{ cm}^{-1}$ , and  $201\text{ cm}^{-1}$ , for Fe/Ni, Ni/Co, and  $\text{LiNi}_{0.5}\text{Co}_{0.5}\text{O}_2$ , respectively. This indicates that the addition of  $\text{LiO}_2$  to the Ni/Co catalyst, results in a shift of the distribution toward smaller diameters. This is true, even when just a sub-set of the total distribution is probed, for fixed experimental conditions and highly homogeneous samples. The positions of the RBMs were assigned to structures of tubes selected using a resonant window around the laser energy. Comparison of calculated and experimental frequencies allowed us to infer that the intertube coupling is weak in the small bundles of the SWCNTs of this work.

## 2. Experimental

The SWCNTs were produced by the arc-discharge method as reported in detail earlier<sup>11</sup>. The anode was a 6.2 mm diameter graphite rod, 100 mm long. A hole with a  $\phi = 2.0$  mm and depth of about 84 mm was drilled into one end. The hole was filled with a catalyst mixture and turned down into the central hole of a copper holder. Three different catalysts were prepared with mixture of selected elements in at % as Fe:Ni (1:1), Ni:Co (1:1) and  $\text{LiNi}_{0.5}\text{Co}_{0.5}\text{O}_2$ . The samples thus obtained will be referred to in this work as FeNi, NiCo and NiCoLi, respectively. An arc was generated between the anode and the graphite cathode at  $\sim 60$  A during the chamber pressure increasing process. The higher current of 100-120 A, was sustained for 15 min to degas the system adequately. A partial atmosphere of high purity helium of 400 torr was used. An initial 1-2 mm gap between the graphite electrodes is opened and several mm were maintained by continuously translating the cathode downward during the arc process. A fairly constant gap voltage (30 V), was established for a constant cathode advance. The advance rate was such as to reduce a 100 mm rod to a stub in about eight minutes. The soot from the collar was chosen as sample because it was found to be richer in SWCNTs than those from the cathode deposit or the interior walls<sup>11</sup>. The growth conditions were strictly the same for all samples.

The Raman spectra were acquired on a T 64 000 Jobin-Yvon triple spectrometer used in the double subtractive configuration. As exciting radiation the 488.0 nm line of an  $\text{Ar}^+$  laser was employed at a low power ( $\sim 100$  mW on the laser output beam) to avoid heating the samples. An OLYMPUS BH-2 microscope allowed for a  $\sim 1\text{ }\mu\text{m}$  spot size to be obtained upon focalization of the laser. The measurements were performed in the backscattering geometry, at room temperature. All measurements were carried out systematically, by fixing the incident power of an  $\text{Ar}^+$  laser line, the scattering geometry and the acquisition parameters. Each sample was measured twice, in different powders, to

check for homogeneity. The spectra reveal just a few differences in intensity of the peaks in different powders of the same sample probed.

## 3. Results and Discussion

The morphology of the samples obtained by the arc-discharge method described above is a high density of SWCNT bundles together with carbon nanoparticles, and many other particles including probably metals and carbide compounds. The bundles of 5 to 11 tubes have diameters of 7 nm to 16 nm and lengths in the scale of  $\mu\text{m}$ . A representative Scanning Electron Microscopy image of a sample produced under similar conditions by using a bimetallic catalyst (FeNi) published earlier<sup>12</sup>, shows amorphous carbon aggregates and other impurities sticking to the bundles.

Figure 1 shows the High Resolution Transmission Electron Microscopy (HRTEM) image of a NiCoLi sample, where the bundles are seen as isolated traces, surprisingly, a very different image from that obtained for the bimetallic catalyst samples. In this case, the image does not show the presence of impurity particles sticking to the bundles or severe amounts of isolated impurities. We thus believe that  $\text{LiO}_2$  play a role by improving the quality of the SWCNTs samples. This higher quality has not been obtained before in any of the as grown soot for any of the most popular catalysts. There are several attempts to explain the SWCNTs properties describing variation of diameters and lengths of

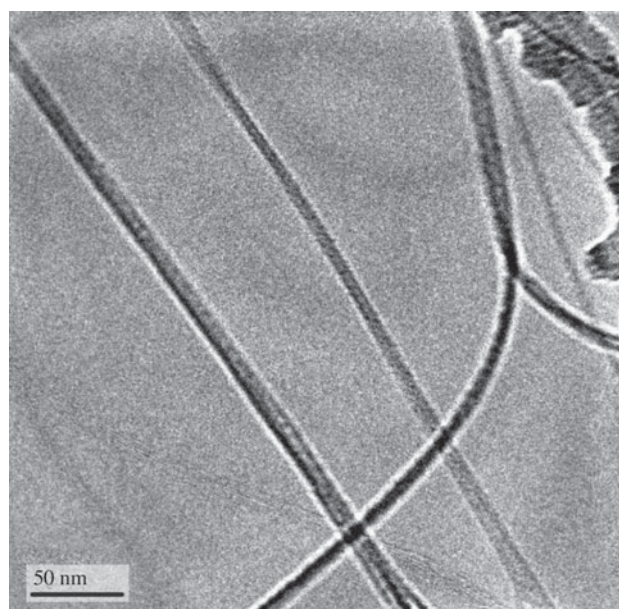


**Figure 1.** High Resolution Transmission Electron Microscopy of SWCNTs produced using the catalyst mixture:  $\text{LiNi}_{0.5}\text{Co}_{0.5}\text{O}_2$  and the arc-discharge method.

the tubes. However, we are unable to find a specific mechanism for the  $\text{LiO}_2$  catalyst to increase the purity of the SWCNTs produced. In fact, the use of a catalyst mixture of three elements makes the situation much more complex. Notice that there are several examples where a bimetallic catalyst is highly efficient in producing SWCNTs while the single metal catalyst is not. This is the case, for instance, of the bimetallic catalyst NiY that is very effective to produce large quantities of SWCNTs in the arc-discharge method and Y is not<sup>6</sup>. The latter can produce only the sea urchin type short tubes and with low yield<sup>6,13</sup>. A possible argument is the increased time in the SWCNTs synthesis in consequence of increased temperature difference between the vaporization and the eutectic formation. This type of argument was used earlier to justify the production of longer bundles<sup>14</sup>. The argument was extended to explain the relationship between the tube diameter and the nature of the catalyst by using the Kanzow and Ding model<sup>15</sup>, in the following way: a small graphene sheet is formed at the surface of a particle. The competition between the kinetic energy of the sheet and the adhesion with the metal particle establish the SWCNTs growth. If the kinetic energy is higher than the work of adhesion, the sheet oscillates and a small cap is formed. From this cap the growth of SWCNTs can start. The larger the difference of the two energies, the smaller the diameter of the tube. Since the kinetic energy depends on the temperature and the work of adhesion depends on the nature of the catalyst, the diameter of SWCNTs depends on both, the catalyst and the temperature. In order to estimate the SWCNTs abundance related to the amount of amorphous carbon in the samples we calculated the Raman intensity ratios between peaks G and D in the tangential modes frequency region (not shown here). We found this ratios to be 4.2, 2.4 and 1.1 for the NiCo, NiCoLi and FeNi samples respectively. This procedure is currently used because the D-band is the Raman active mode of the defective carbon network<sup>6,7</sup>. The G/D value is a reasonable good abundance index in the present situation for, the laser excitation lying in the semiconductor resonance window, the metallic tubes do not contribute to the G peak shape.

The average diameter of the SWCNTs in the bundles produced by using the Ni/Co/LiO<sub>2</sub> catalyst mixture was estimated by using HRTEM techniques. Figure 2 illustrate one such measurement. The solid line in this figure shows a segment of a bundle with 5 tubes and 7.0 nm of length. The number of tubes varies up to 11, in a bundle with 16.5 nm of length. The mean diameter of tubes in this sample was found to be  $\langle d \rangle = 1.46$  nm using the HRTEM results. The same type of measurement gives for FeNi SWCNTs a mean diameter of  $\langle d \rangle = 1.53$  nm (not shown here).

Raman spectra in the radial breathing mode (RBM) range, for the three different samples measured are shown in Fig. 3. The upper curve corresponds to the SWCNTs pro-

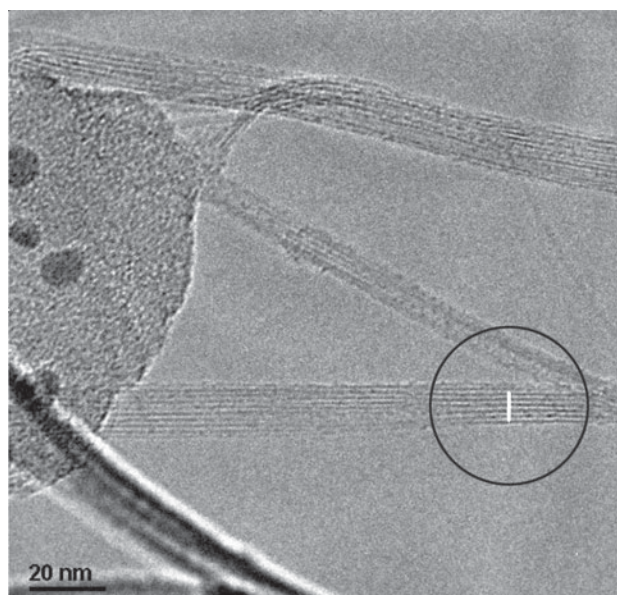


**Figure 2.** High magnification HRTEM image of SWCNTs produced using the catalyst mixture:  $\text{LiNi}_{0.5}\text{Co}_{0.5}\text{O}_2$  and the arc-discharge method.

duced with the  $\text{LiNi}_{0.5}\text{Co}_{0.5}\text{O}_2$  catalyst mixture. The Raman intensity peaks at  $201.5\text{ cm}^{-1}$ . The intermediate curve in this figure represents the tubes grown with the bimetallic catalyst NiCo. The Raman structure in this case is broader, peaks at  $179.9\text{ cm}^{-1}$  and is shifted toward lower frequencies. The lowest curve in Fig. 3 is the spectrum for the SWCNTs obtained by using the FeNi catalyst. The Raman intensity has one maximum at  $158.2\text{ cm}^{-1}$  and the overall structure is shifted toward lower frequencies as compared to the previously described spectra. The position of the Raman RBMs do not allow to define directly the distribution of diameters in the SWCNTs samples, but probe just a sub-set of nanotubes which are in resonance either with the incident or the scattered photon, as pointed out earlier<sup>16</sup>. However, it can give a scaling of mean diameter when the several SWCNTs samples are homogenous. This is the case of the three samples of this work, for which the Raman spectra obtained from different spots in the sample were the same. Hence, the Raman RBMs spectra shown in Fig. 3 indicates that the mean diameter follows a relation given by:  $\text{FeNi} > \text{NiCo} > \text{NiCoLi}$ . The reason for the decrease in the nanotube diameter may be similar to that described earlier<sup>14</sup>, for the role of a Ni/Co/S mixture catalyst as compared to the single metallic catalysts. The role of the additional element, S, was proposed to be the decrease of the eutectic temperature in the carbon-nickel-cobalt system and also a small decrease of the temperature in the condensing zone. The lower formation temperature induces the formation of

**Table 1.** Chiralities for nanotubes, calculated diameter,  $d$ , resonant energy,  $2.44 \text{ eV} < E < 2.64 \text{ eV}$ , calculated frequency,  $\omega$ , and Raman frequencies,  $\omega_x$ . Here,  $\omega = \alpha/d$ , with  $\alpha = 248 \text{ cm}^{-1} \text{ nm}$ .

(m,n)	$d$ (nm)	$E$ (eV)	$\omega$ ( $\text{cm}^{-1}$ )	$\omega_x$ ( $\text{cm}^{-1}$ ) FeNi	$\omega_x$ ( $\text{cm}^{-1}$ ) NiCo	$\omega_x$ ( $\text{cm}^{-1}$ ) NiCoLi
(10,8)	1.24	2.63	200.0			201.5
(11,7)	1.25	2.52	198.4	197.3	196.5	195.7
(10,9)	1.31	2.45	189.3		190.8	189.7
(12,7)	1.32	2.52	187.9			
(17,0)	1.35	2.62	183.7			
(16,2)	1.36	2.59	182.3			
(15,4)	1.38	2.51	179.7	179.9	179.9	180.8
(11,10)	1.44	2.64	172.2	172.6	172.3	
(17,3)	1.48	2.55	167.6		166.1	
(12,10)	1.51	2.62	164.2			
(15,7)	1.55	2.51	158.3	158.2	158.5	
(12,11)	1.58	2.56	157.0			
(14,9)	1.59	2.47	156.0			
(15,8)	1.61	2.61	154.0			
(14,10)	1.66	2.48	149.4	149.0		

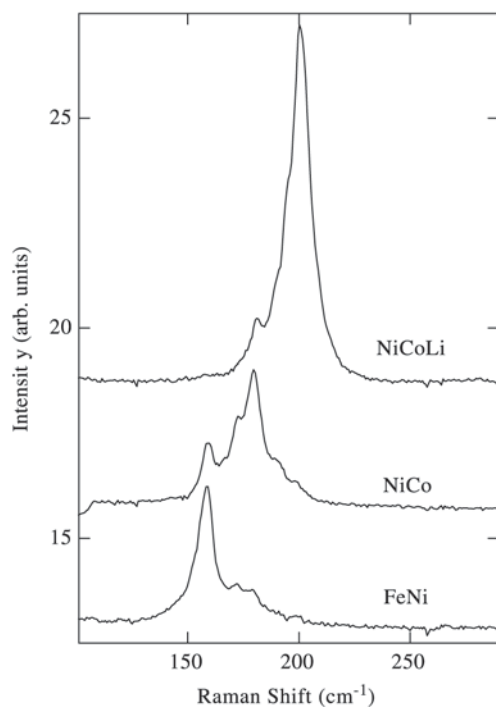


**Figure 3.** Raman spectra from three different SWCNTs samples in the radial breathing mode frequency range.

narrower tubes, and the subsequent increase of temperature range in the growth area favors the increase of the length of the tube<sup>14</sup>.

It should be noticed that there is an alternative proce-

dure to obtain the mean diameter using Raman scattering, as proposed by Corio *et al.*<sup>16</sup>, relating the diameter distribution to the tangential modes. This kind of procedure cannot be used here, because it applies to metallic nanotubes, in resonance with the lowest electronic transition energy ( $E_{11}$ ). By using a higher excitation energy,  $E_1 = 2.54 \text{ eV}$ , we selected another resonant window corresponding to energy separation  $E_{ii}$  ( $i = 3,4$ ) between van Hove singularities for semiconductor nanotubes. This can be checked by the analysis of the plots  $E_{ii}$  versus nanotube diameters, as found in the work of Jorio *et al.*<sup>17</sup> (Fig. 3). We use RBM frequencies for a tentative assignment of the (n,m) parameters of the tubes, as listed in Table 1. The table lists the possible (n,m) values in the first column, for the selected energy window ( $2.44 \text{ eV} < E_{ii} < 2.64 \text{ eV}$ ).

The discrete set of helicities for the tubes was determined from the joint density of states calculation associated to an *ab initio* simulation of resonance Raman response<sup>18</sup>. The main parameters entering this evaluation are the matrix element,  $\gamma$ , and the excited state lifetime,  $\tau$ . The values found appropriate for those quantities are  $\gamma = 2.9 \text{ eV}$  and  $\hbar/(2\pi\tau) = 0.01 \text{ eV}$ , respectively, with  $\hbar$  being the Planck's constant.

The second column of the table lists the diameters calculated through the relation:

$$d = (m^2 + nm + n^2)^{1/2} (\sqrt{3}/\pi) a_{cc}, \quad (1)$$

where  $a_{cc}$  is the C-C spacing in carbon nanotubes. The resonant energies in the selected window are listed in the third column of Table 1. The fourth column lists the frequency

values given as the ratio  $\alpha/d$ , with  $\alpha = 248 \text{ cm}^{-1} \text{ nm}$ . The last three columns are Raman frequencies measured in this experiment. The value of  $\alpha$  chosen here is the same as that used for the determination of structure of isolated tubes<sup>17</sup>. The reason for this choice is that the agreement between calculated and measured frequencies fall within the experimental accuracy of  $2 \text{ cm}^{-1}$ . This agreement is probably an indication that the intertube coupling in the bundles are quite negligible for our samples, probably due to the small amount of tubes in each bundle. It should be said that neither the use of the  $\alpha$ -value introduced by Bandow *et al.*<sup>19</sup> or other calculated frequencies taking into account intertube coupling corrections, as proposed recently by Rao *et al.*<sup>20</sup>, compared to our experimental results with such a good agreement. Table 1 also shows the same scaling in the sub-set diameter distribution as that observed for the mean diameter obtained through HRTEM: FeNi > NiCo > NiCoLi. Moreover, the sub-set mean diameter is smaller than that measured for the complete distribution. This is understandable considering that the higher diameter semiconductor nanotubes are not observed here due to a weaker resonance with the higher order transition energy  $E_{44}$  than that with the  $E_{33}$  energy.

#### 4. Conclusion

The arc-discharge method was used to produce three different SWCNTs using different catalyst mixtures, Fe/Ni, Ni/Co, and Ni/Co/LiO<sub>2</sub>. The SWCNTs were characterized by using HRTEM and Raman spectroscopy. HRTEM shows that the bimetallic Fe/Ni catalyst produced SWCNTs with impurities sticking to them, while the use of a Ni/Co/LiO<sub>2</sub> mixture catalyst leads to impurity free SWCNTs. Among the three samples, NiCo was determined as the most SWCNTs abundant. Both measurements show one scaling of nanotubes diameters, in qualitative agreement, as follows: FeNi > NiCo > NiCoLi. Possible chiralities are predicted for semiconductor nanotubes and tentative assignments of the observed frequencies are presented.

#### Acknowledgements

The authors thank Dr. A.G. Souza Filho for helpful discussions, and the staff of Laboratório Nacional de Luz Síncrotron, LNLS, for help with the use of the HRTEM equipment (JEOL JEM 3010). Financial support from Conselho Nacional de Desenvolvimento Científico e Tecnológico, CNPq, and Fundação de Amparo à Pesquisa do Estado de São Paulo, FAPESP, are greatly acknowledge.

#### References

- Iijima, S.; Ichihashi, T. *Nature* 363 (6430), p. 603-605, 1993; *ibid* 364 (6439), p. 737-737, 1993.
- Bethune, D.S.; Kiang, C.H.; de Vries M.S.; Gorman, G.; Savoy, R.; Vazquez, J.; Beyers, R. *Nature* 363 (6430), p. 605-607, 1993.
- Saito, Y.; Yoshikawa, T.; Okuda, M.; Fujimoto, N.; Simiyama, K.; Suzuki, S.; Kasuyas, A.; Nishima, Y. *J. Phys. Chem. Solids* 54 (12), p. 1849-1860, 1993.
- Thess, A.; Lee, R.; Nikolaev, P.; Dai, H.; Petit, P.; Robert, J.; Xu, C.; Lee, Y.H.; Kim, S.G.; Rinzler, A.G.; Colbert, D.T.; Scuseria, G.E.; Tománek, D.; Fisher, J.E.; Smalley, R.E.; *Science* 273 (5274), p. 483-487, 1996.
- Hafner, J.H.; Bronikowski, M.J.; Azamian, B.R.; Nikolaev, P.; Rinzler, A.G.; Colbert, D.T.; Smith, K.A.; Smalley, R.E. *Chem. Phys. Lett.*, 296 (1-2), p. 195-202, 1998.
- Takizawa, M.; Bandow, S.; Yudasaka, M.; Ando, Y.; Shimoyama, H.; Iijima, S. *Chem. Phys. Lett.* 326 (3-4), p. 351-357, 2000.
- Kataura, H.; Kumazawa, Y.; Maniwa, Y.; Ohtsuka, Y.; Sen, R.; Suzuki, S.; Achiba, Y. *Carbon* 38 (11-12), p. 1691-1697, 2000.
- Seraphin, S.; Zhou, D. *Appl. Phys. Lett.* 64 (16), p. 2087-2089, 1994.
- Saito, Y.; Tani, Y.; Miyagawa, N.; Mitsushima, K.; Kasuya, A.; Nishima, Y. *Chem. Phys. Lett.* 294 (6), p. 593-598, 1998.
- Journet, C.; Maser, N.K.; Bernie, P.; Loiseau, A.; de la Chapelle, M.L.; Lefrant, S.; Deniard, P.; Lee, R.; Fischer, J.E. *Nature* 388 (6644), p. 756-758, 1997.
- Huber, J.G.; Romero, J.V.; Spivey, J.D.; Luengo, C.A. *Química Nova*, 24 (6), p. 898-900, 2001.
- Romero, J.V.; Luengo, C.A.; Huber, J.G.; Rosolen, J.M. *Química Nova*, 25 (1), p. 59-61, 2002.
- Zhou, D.; Seraphin, S.; Wang, S. *Appl. Phys. Lett.* 65 (12), p. 1593-1596, 1994.
- Alvarez, L.; Guillard, T.; Sauvajol, J.L.; Flamant, G.; Laplaze, D. *Chem. Phys. Lett.* 342 (1-2), p. 7-14, 2001.
- Kanzow, H.; Ding, A. *Phys. Rev. B* 60 (15), p. 11180-11186, 1999.
- Corio, P.; Temperini, M.L.A.; Santos, P.S.; Romero, J.V.; Huber, J.G.; Luengo, C.A.; Brown, S.D.M.; Dressehaus, M.; Dressehaus, G.; Dantas, M.S.S.; Leite, C.F.; Matinaga, F.; Gonzalez, J.C.; Pimenta, M.A. *Chem. Phys. Lett.*, 350 (5-6), p. 373-380, 2001.
- Jorio, A.; Saito, R.; Hafner, J.H.; Lieber, C.M.; Hunter, M.; McClure, T.; Dressehaus, M.; Dressehaus, G. *Phys. Rev. Lett.* 86 (6), p.118-1121, 2001.
- Milnera, M.; Kürti, J.; Hulman, M.; Kuzmany, H. *Phys. Rev. Lett.* 84 (6), p. 1324-1327, 2000 and references therein.
- Bandow, S.; Asaka, S.; Saito, Y.; Rao, A.M.; Grigorian, L.; Richter, E.; Eklund, P.C. *Phys. Rev. Lett.* 80 (17), p. 3779-3782, 1998.
- Rao, A.M.; Chen, J.; Richter, E.; Schlecht, U.; Eklund, P.C.; Haddon, R.C.; Venkaterwaran, U.D.; Lwon, Y.-K.; Tomanek, D. *Phys. Rev. Lett.* 86 (17), p. 3895-3898, 2001.